

A 25nN Low-Noise Thrust Stand for Microthrusters

Claude R. Phipps* and James R. Luke†
Photonic Associates, LLC, Santa Fe, NM 87508

Wesley D. Helgeson‡
NMT/IERA, Albuquerque, NM 87106

We describe the design, construction, testing and calibration of a microthruster thrust stand capable of 25nN thrust resolution. The test stand can carry a fully operational microthruster and power supply with up to 15kg total mass. Thrust capacity is 500μN with 0.5% accuracy. Minimum response with 25% accuracy is 100nN. The thrust stand is a critically-damped torsion balance with 80-s period, for which thrust is proportional to rotation angle. The trick is to measure rotation angle with 20μrad resolution, and we do that with an interferometer design which is sensitive only to rotation, not translation. This feature eliminates sensitivity to ambient vibration. Advantages of this design are that thrust readout noise is essentially absent for frequencies above 0.1Hz, only minimal balancing of the load is required, and response to ambient mechanical noise, such as is produced by footsteps, nearby vacuum pumps, etc., is eliminated. Torsion produced by a magnetic dipole was used for calibration. We will present typical thrust data obtained with the device and a movie showing the readout in operation.

Key words: nN force measurement, rotational interferometer, thrust stand, microthruster

Nomenclature

a_1	= radius of small Helmholtz coil	Q^*	= specific ablation energy
a_2	= radius of large Helmholtz coil	R	= radius of thruster attachment point from center of rotation
B	= magnetic field intensity	v_E	= exhaust velocity
C_m	= laser momentum coupling coefficient	T	= torque
CW	= “continuous wave”, continuous laser output rather than pulsed	W	= laser pulse energy incident on test sample
d	= diameter of torsion fiber	Δm	= ablated mass
E	= short for “10 [^] ”	η_{AB}	= ablation efficiency
f	= repetition frequency	μ_o	= permeability of free space
F	= thrust	θ	= angle of rotation of torsion bar
G	= torsion modulus of pendulum fiber	τ	= laser pulse duration
g_o	= acceleration of gravity at Earth’s surface		
I	= laser intensity on target		
J	= polar moment of inertia of torsion fiber		
I_{sp}	= specific impulse		
k	= constant relating rotation angle θ to torque		
L	= length of torsion fiber		
m	= magnetic dipole moment		
N_1	= number of turns, small calibration coil		
N_2	= number of turns, large calibration coil		
$\langle P \rangle$	= average incident laser power		

* President and General Partner, 200A Ojo de la Vaca Road, crhipps@aol.com. Member AIAA.

† Senior Research Staff Member and Partner, 200A Ojo de la Vaca Road.

‡ Senior Research Associate, 901 University Blvd SE.

I. Introduction

We were forced to redesign our thrust stand [1] by the requirement of measuring thrust with sub-100nN-level precision in a recent project [2]. Simulations done to prepare for these ns-pulse microthruster feasibility demonstrations showed that, in the laser fluence regime of interest for tests driven by a microchip laser [100-300 kJ/m²], C_m was expected to be in the range 10 - 100 μ N/W. With $P = 106$ mW delivered through the target illumination train to the target by our Concepts Research, Inc. model CRLB-0001-1064 “microchip” laser used for some of the target interaction tests, thrust as small as 1.1 μ N needed to be measured with 2% accuracy, meaning that we ideally needed 25nN measurement precision. The lower end of the range of interest would be achieved by attenuating the laser, resulting in thrusts as small as 300nN, measurements for which good precision was even more important.

Smaller forces are, of course, easily measured in a device that doesn't have to carry this much mass. Our small torsion pendulum, intended for target sample qualification, can measure forces as small as 4nN, but its carrying capacity is just 10 grams [3].

After considering alternatives, we chose to stay with the torsion pendulum as a basic design, but to improve our rotation angle resolution. At first, we tried to do this by creating a Mach-Zehnder interferometer incorporating a corner-cube retroreflector attached to the end of the torsion bar inside the test chamber as one mirror, with the other three optics situated on the optical table outside the vacuum test chamber. After equalizing paths and determining that the coherence length of our probe laser matched the expected change of optical path length during thrust measurements, we found two disadvantages with this technique. First, the 2 μ rad rotation resolution (corresponding to 3nN) was an order of magnitude greater than the 20 μ rad which we required to resolve 25nN. Second, any vibration, especially the 140 Hz input from the spinning target holder which was part of the ns-pulse μ thruster mounted on the torsion bar, totally erased the interference fringes we were observing.

We settled on an optical readout design that gave just the required resolution and is sensitive only to rotation, not translation. The result could well tolerate the spinning target disk mounted directly on the thrust stand, and environmental inputs such as laboratory foot traffic and floor-mounted rotating forepumps.

II. Definition of Terms

For the sake of simplicity, we will consider a monoenergetic laser-produced plasma jet with exhaust velocity v_E . We have shown that this approximation will not introduce large errors [$\langle v^2 \rangle / \langle v \rangle^2 \approx 1.15$] for typical laser-produced plasma jets, and the principal points we want to make here will be made more transparently using that assumption. We define the laser momentum coupling coefficient C_m as:

$$C_m = F / \langle P \rangle = \Delta m v_E / W. \quad (1)$$

In the ablation process, Q^* joules of laser light are consumed per kg of ablated mass, and C_m units of impulse $\Delta m v_E$ are produced. The product of C_m and Q^* is the exhaust velocity v_E of the ablation stream, given the monoenergetic assumption. This can be seen from the definitions of C_m and Q^* :

$$C_m Q^* = (\Delta m v_E / W)(W / \Delta m) = v_E, \quad (2)$$

independent of the ablation efficiency. If for example, a significant amount of the incident energy is absorbed as heat in the target substrate rather than producing material ejection, Q^* will be higher, but C_m will be proportionately lower, giving the same velocity in the end. In propulsion work, “specific impulse” I_{sp} is customary notation for v_E / g_0 , and we define I_{sp} as

$$I_{sp} = C_m Q^* / g_0. \quad (3)$$

Energy conservation prevents C_m and I_{sp} from being arbitrary. Increasing one decreases the other. Energy conservation requires that several constant product relationships exist:

$$2\eta_{AB} = \Delta m v_E^2 / W = C_m^2 Q^* = g_0 C_m I_{sp} = C_m v_E. \quad (4)$$

The ablation efficiency parameter η_{AB} in Eq. (3) is the ratio of exhaust kinetic power to incident laser power $\langle P \rangle$. The definition allows $\eta_{AB} > 1$ for exothermic targets. For nonexothermic “passive” targets, $\eta_{AB} \leq 1$ and the product

$$C_m I_{sp} \leq 2/g_0 = 0.204. \quad (5)$$

III. Thrust Stand Design

Figure 1 shows the vacuum thrust stand setup. It is identical to the thrust stand reported in [1] except for a) 40-cm rather than 10-cm torsion fiber length, b) the critical damping attachment and c) the interferometer element in the center of the support bar. The latter replaces the simple mirror used as a rotation readout in [1]. The entire setup mounts inside the vacuum test chamber.

Thrust F is given by

$$F = k\theta/R \quad (6)$$

Where

$$k = GJ/L = \pi d^4 G / (32L) \quad (7)$$

In our case, $k = 194 \text{ pN}\cdot\text{m}/\mu\text{rad}$ and $R = 0.155\text{m}$, so that $k/R = 1.25\text{nN}/\text{mrad}$. For the thrust stand to have 25nN

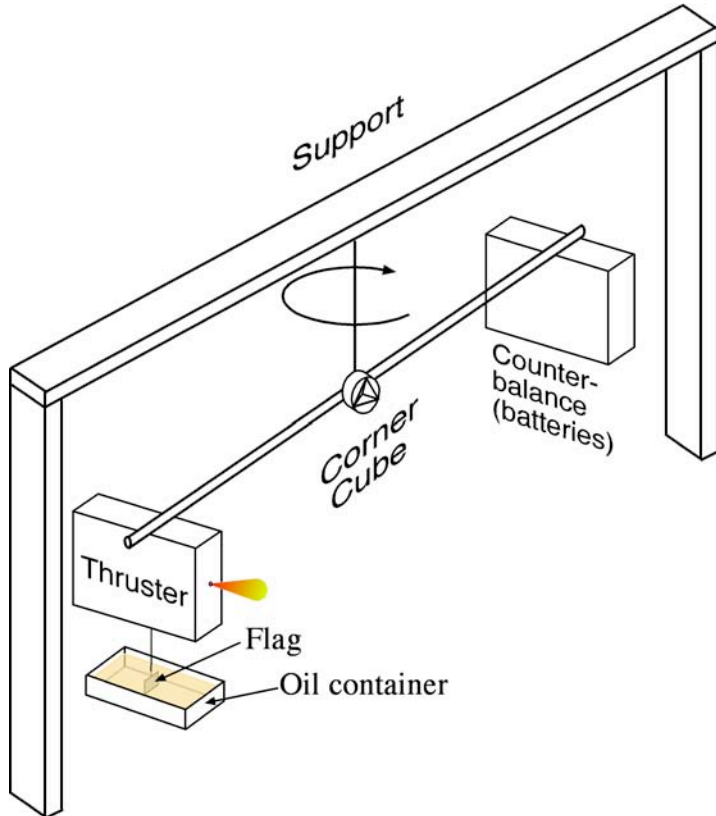


Figure 1. Vacuum thrust stand setup. Power supply is on board the thrust measurement bar with the thruster, and command and data transfer uses an IR data link, so that the only mechanical connection with the outside world is the 254- μm diameter steel fiber supporting the bar. An interferometer based on a solid glass retroreflecting “corner cube” (described below) is the key to resolving rotation of the bar. Critical damping is provided by a flag immersed in diffusion pump oil.

precision, the rotation sensor must resolve 20 μrad bar rotation.

To measure rotation of the torsion bar, we developed a new type of optical interferometer not previously reported in the literature [Figures 2A and 2B]. The retroreflector has 2.54cm diameter aperture. Beam (1) in Figure 2 is a 5mW, 532-nm near-diffraction-limited CW beam expanded to 15mm collimated diameter using a beam expansion telescope. The torsion bar is suspended from a 254- μm diameter steel fiber. In Figure 2A, this attachment point is indicated as S, and the microthruster applies thrust at point F. A solid glass “corner cube” retroreflector prism P is mounted to the bar close to the center. Beam (1) strikes the corner cube and produces two reflected beams (2) and (6). The initial angle between beam (1) and beams (2) and (6) is adjusted to about 30mrad to optimize sensor performance. These interfere on a screen, producing the fringes shown in the inset. As rotation occurs, these fringes move radially outward (as illustrated by the arrows in the inset) or inward, depending on the direction of rotation of the bar. Counting the passage of the fringes, which can be done visually or using the figure 3 setup, gives rotation.

The origin of beam (6), which results from two internal roundtrips through the prism, is illustrated in greater detail in Figure 2B. The corner cube prism is a solid glass object with vertices (A), (B), (C) and (D). The angles made by the edges at (D) are all 90 degrees, hence “corner cube”.

Beam (1) strikes the front face ABC producing the reflected beam (2). It also passes through the uncoated prism face and, after two internal reflections, produces external beam (4) which is exactly antiparallel to beam (1). Generation of beam (4) is the normal application of a corner cube. However, beam (4) also reflects internally off face ABC, producing beam (5) which, after two internal reflections, produces external beam (6). Beam (6) is precisely parallel to beam (2), independent of the cube orientation to beam (1). The phase difference between the beams (2) and (6) varies as the prism is rotated with respect to beam (1) due to small, angle-dependent differences between the total path length of beams (2) and (6), producing the interference fringes which are the basis of the rotation measurement.

The retroreflector function resembles that of a simple planar etalon in some ways, but there are important differences in detail.

First, because of the complex internal optical path, the prism is ten or more times as effective in creating optical path difference compared to an etalon with the same thickness as the prism depth.

Second, unlike an etalon, for which the phase shift is quadratic with incidence angle, the fringe shift in the prism is absolutely linear with rotation [Figure 4].

Quadratic phase shift leads to calibration constants and sensitivity which must be specified separately with each new incidence angle.

Linear phase shift is a unique advantage of the prism, making absolute calibration possible.

Also plotted in Figure 4 is the response of a planar etalon having the same thickness as the prism depth and equal refractive index.

Table 1 summarizes the device performance, and compares it to the performance obtained with a mirror rather than an interferometer located at the torsion bar center of rotation, which we used in [1]. Although only 2.5 cm in diameter, the prism has the same angular resolution ($20\mu\text{rad}$) as the diffraction-limited beamwidth of a 6.5-cm diameter optic at its 532 nm operating wavelength.

To appreciate how small the resolved forces are, consider the C_{mhv} of reflected light (no ablation), 6.7nN/W . With our balance, the pressure of a 4W collimated light beam should just be measurable. Also, the gravitational attraction of the experimenter standing 50cm from the microthruster should also be barely observable, although well beneath the noise level of the device. We did not do either of these measurements, due to lack of a good collimated 4W laser source in the first instance, and to inadequate sensitivity for a believable measurement in the second.

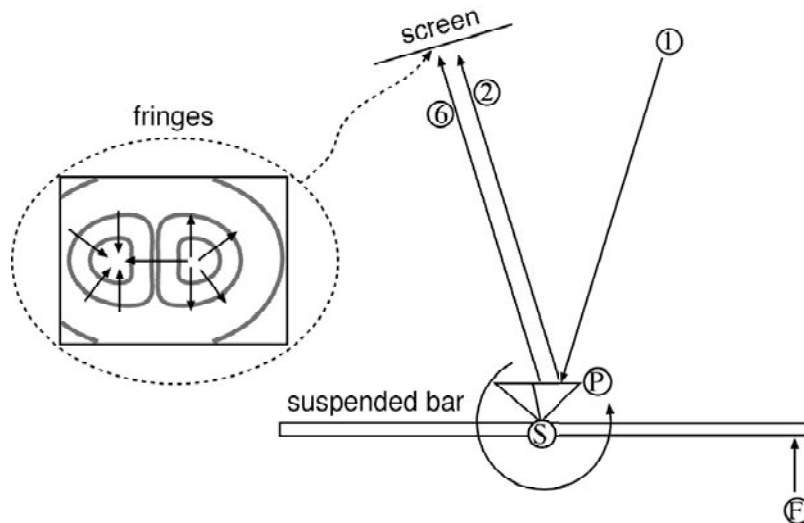


Figure 2A. Schematic of torsion bar rotation interferometer, viewed from above.

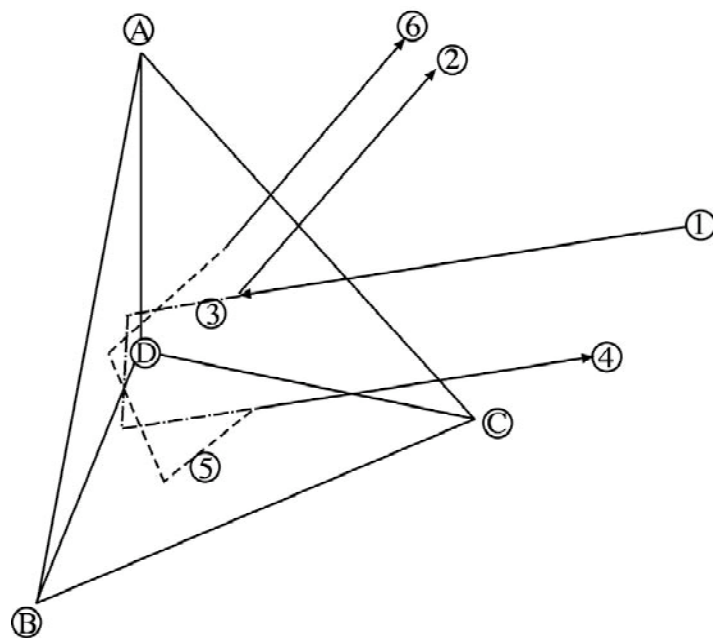


Figure 2B. Illustrating the origin of beams (2) and (6) in Figure 2A.

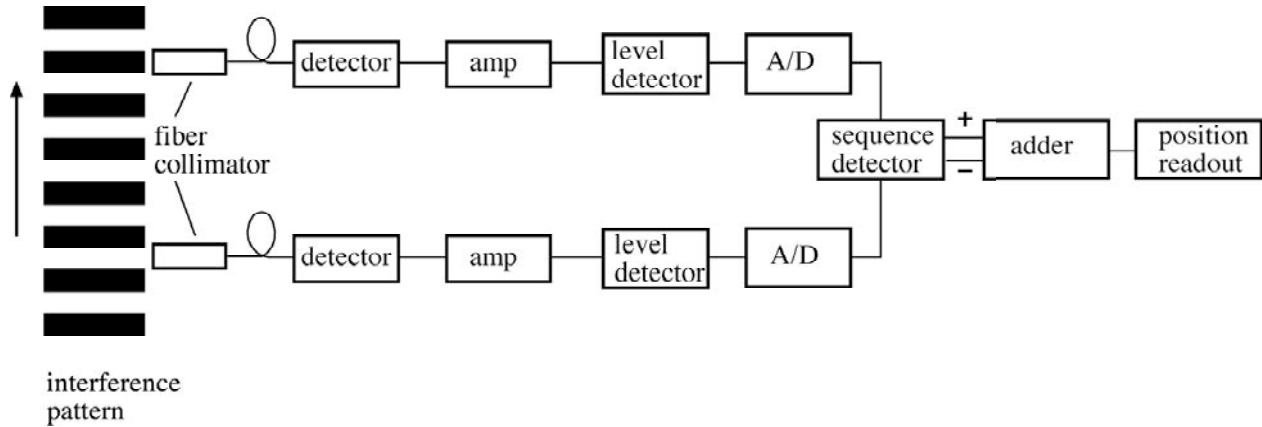


Figure 3. Fringe-counting electronics

Parameter	Value
Prism diameter (cm)	2.54
Prism depth (cm)	0.90
Sensor response ($\mu\text{rad}/\text{fringe}$)	136.6
Force response ($\text{nN}/\mu\text{rad}$)	1.25
Force response (nN/fringe)	171
Maximum thrust measurable [using interferometer] (μN)	100
Minimum thrust measurable with 25% precision [using interferometer] (nN)	100
Minimum angular resolution (μrad)	20
Corresponding precision (nN)	25
Maximum thrust measurable [using conventional mirror] (μN)	500
Minimum thrust measurable with 25% precision [using conventional mirror] (μN)	8
Precision with conventional mirror (μN)	2
Load capacity (kg)	15

IV. Interferometer Calibration and Test

Torsion balance calibration was based on the magnetic torque between a large, fixed Helmholtz coil and a small, centered rotatable Helmholtz coil attached to the torsion bar. This is a primary calibration. The procedure is described in more detail in [1].

For the two coils (a_2 and a_1 are the radii of the large and small coils, respectively), the torque T is

$$T = mB = \frac{\mu_0 \pi a_1^2}{2a_2} i_1 i_2 N_1 N_2 \quad (8)$$

We used $N_1=20$ and $N_2=300$. We measured the pendulum rotation vs. combinations of i_1 and i_2 with $a_2=0.219\text{m} \gg a_1=0.039\text{m}$ to determine, for the case where the torsion fiber was 10cm long, $T = 774 \mu\text{N}\cdot\text{m}/\text{rad} \pm 10\%$. We then extended the torsion fiber length to 40cm for these measurements, and calculated

$$T = 194 \mu\text{N}\cdot\text{m}/\text{rad} \pm 10\% . \quad (9)$$

With $R = 15.5 \text{ cm}$, the thrust response of the device becomes

$$F = 1.25 \text{ nN}/\mu\text{rad} , \quad (10)$$

as indicated in Table 1. The sensor calibration is shown in Figure 4, where its response is compared to that of an etalon of the same depth, both at 30mrad initial incidence angle.

Figure 5 shows an example of data taken on our ns-pulse microthruster with the test stand we have described.

V. Conclusions

We built and tested a torsion balance thrust stand with 25nN precision, capacity from 100nN to 500 μN and mass capacity 15kg. The thrust stand's optical rotation readout is a new type of interferometer, 2.5 cm in diameter, which responds only to rotation, not translation and has 20 μrad rotational resolution.

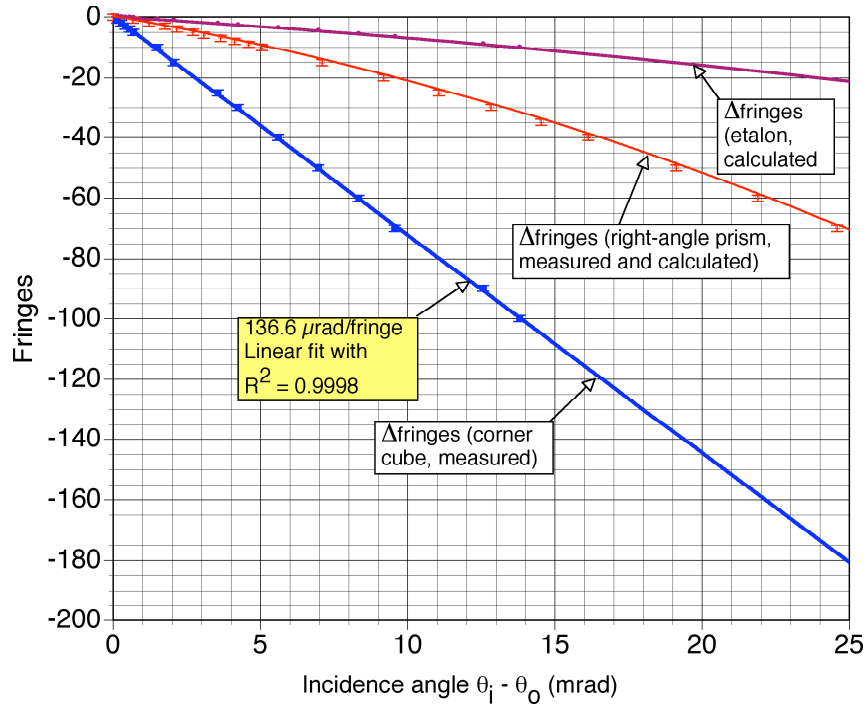


Figure 4. Calibration curve for the corner cube compared to that calculated for an etalon and a right-angle prism of similar depth. A zero-fringe incidence angle of 30mrad is assumed for the etalon calculation. At this angle, the prism is ten times more effective than the etalon, and its response is linear at any incidence angle.

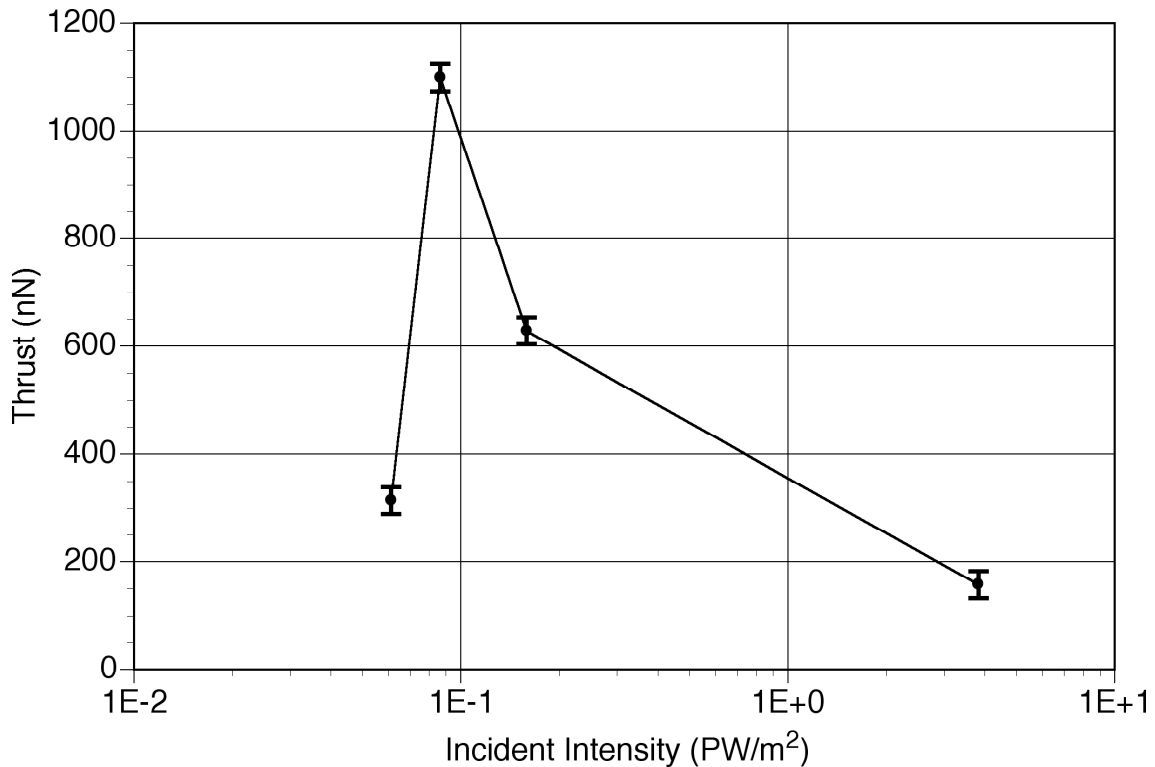


Figure 5. Thrust vs. intensity for ns-pulse microthruster obtained with the 25nN torsion balance. These data were obtained with a Quantel repetitively-pulsed laser delivering $\langle P \rangle = 10 - 12\text{mW}$, $f = 10\text{Hz}$, $\tau = 4.5\text{ns}$, gold target.

References

1. Phipps, C. , Luke, J., Lippert, T., Hauer, M. and Wokaun, A., "Micropropulsion using a Laser Ablation Jet," *J. Propulsion and Power*, **20** no. 6, 2004, pp. 1000-1011
2. C. R. Phipps, "Precision Propulsion Concepts for Microsatellites," SBIR Phase I Final Report, TR-2005-0028, available from AFRL/PRS, 1 Pollux Drive, Edwards AFB, CA 93524-7048
3. Phipps, C. R. and Luke, J. R., "Diode Laser-driven Microthrusters: A new departure for micropropulsion," *AIAA Journal* **40** no. 2 2002, pp. 310-318